ALMA Memo 622

Cross-Polarization and Beam Offsets Due to Optics Element Misalignment

ALMA Band-6 Cartridge

Sivasankaran Srikanth

Central Development Laboratory, NRAO, Charlottesville

November 10, 2022.

Abstract: The Central Development Laboratory (CDL) has been approved in 2022 for upgrading the ALMA Band-6 (211-275 GHz) receiver cartridge with an improved version, referred to as "Band-6v2". The deliverable is a pre-prototype receiver with near quantum-limited noise performance and ultra-wide IF band. This receiver will have lower noise temperature over a wider bandwidth (211-280 GHz), smaller variation in gain and IF power density across the 2-GHz basebands, increased IF bandwidth of 12 GHz or 16 GHz and improved cross-polarization and sidelobe levels. The sources of cross-polarization of the cartridge are the orthomode transducer (OMT), the feed horn, the quasi-optical elements and the vacuum and IR windows. Three new designs of OMT have been analyzed and the plan is to fabricate and make careful measurements to select the best. The OMT section is not covered in this memo. Gaussian beam propagation through the quasi-optics has been analyzed. Cross-polarization levels are computed for cases of misaligned optical elements. Misalignment includes linear translations and rotations from nominal positions. The shift in cartridge beam direction and levels of cross-polarization are shown.

Introduction:

The long term development strategy for the upgrade of hardware, software and analysis tools to enhance observing capabilities of ALMA is detailed in [1]. Reference [2] defines the system level technical goals to guide development efforts for the front-end and digitizer. The current development priorities are to broaden the receiver intermediate frequency (IF) bandwidth by at least a factor of two and to upgrade the associated electronics and correlator to handle the increased bandwidth. A proposal [3] to upgrade the ALMA Band-6 (211-275 GHz) receiver cartridge shown in Figure 1(a) with an improved version, was submitted to the ALMA Board by the CDL in August 2021 and was approved for funding in 2022. The new cartridge referred to as "Band-6v2" will rectify the shortcomings of the current receiver cartridge. Band-6v2 cartridge will have an expanded RF band of 211-280 GHz, reduced and flatter noise temperature across the full IF band, improved receiver gain variation and IF power density slope across the 2-GHz IF bands in the cryogenic electronics and lower sideband noise from LO modules on the warm cartridge assembly. The proposal also calls for improved cross-polarization, lower sidelobe levels and reducing/eliminating the sharp resonances observed in some cartridges at ~230 GHz. In addition, it is also proposed to increase the IF bandwidth to 12 GHz (4-16 GHz) or 16 GHz (4-20 GHz).

In an attempt to lower the cross-polarization levels, the CDL is in the process of evaluating three new designs of the orthomode transducer (OMT). The source of resonance near 230 GHz has been identified and the throat section of the feed horn has been modified. An investigation into the effects of misalignment of the optical elements on cross-polarization levels and beam offsets is presented in this memo.

Gaussian Beam Propagation:

The specified illumination taper at the edge of the subreflector (3.58°) of the ALMA 12m- antenna is -12 dB. At 243 GHz, this translates to a beam waist radius (w_{cass}) of 7.449 mm at the Cassegrain focus. A feed horn with an aperture diameter of 23 mm and length of 150 mm is required to generate such a narrow beam. In order to reduce the length of the cartridge, a moderate size corrugated feed horn and a pair of refocusing mirrors are used. The diameter at the aperture and length of the feed horn are 7.090 mm and 40.739 mm, respectively, and the semi-flare angle is 4.35°. The waist radius (w_0) of the horn is given by equation (1), where a is the aperture radius and R_h is the slant length of the horn. Equation (2) gives the location of the waist z_0 with respect to the aperture of the horn. At 243 GHz, w_0 is 2.192 mm and z_0 is -3.464 mm. A pair of ellipsoidal mirrors are used to transform the waist of the feed horn to the Cassegrain waist. Figure 1(a) shows the arrangement of the mirrors. Table 1 lists the parameters of the Gaussian beam at three frequencies. The parameters of the optical elements are also shown. Some of the parameters such as distances and angles in Table 1 are shown in Figure 1(b).

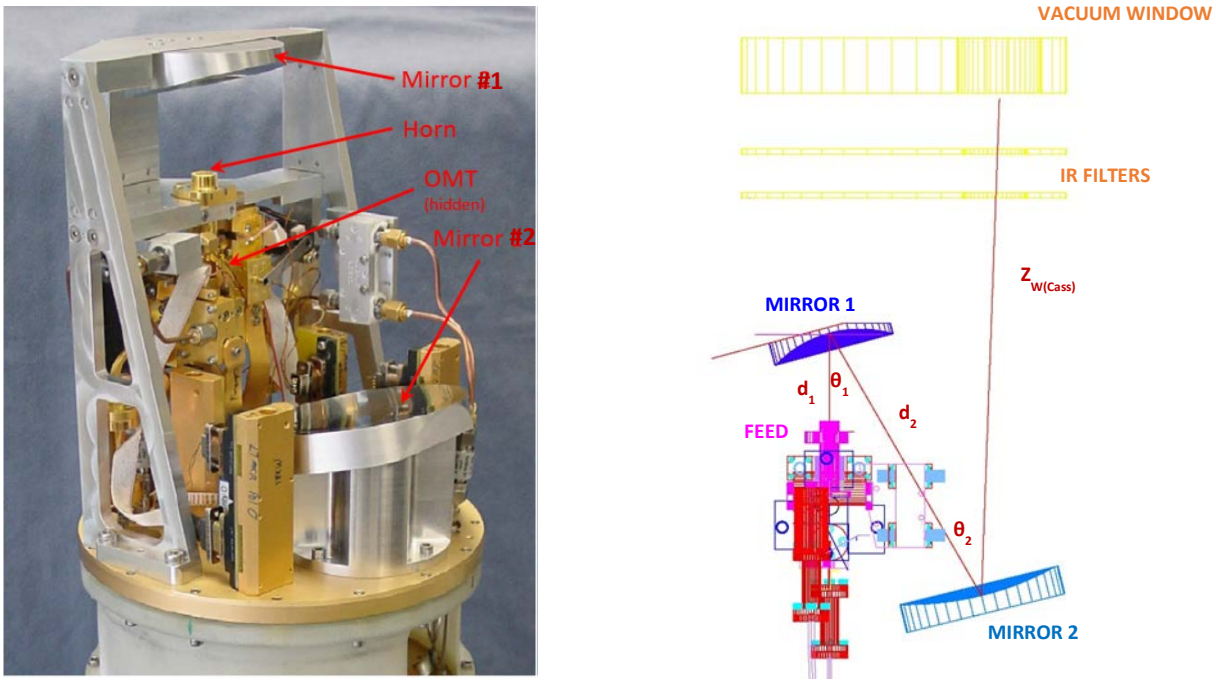

(a) (b)

Figure 1. (a) Photograph of the cartridge, (b) Optical path through the quasi-optics.

$$w_0 = \frac{0.644a}{\left[1 + \left\{\frac{\pi(0.644a)^2}{\lambda R_h}\right\}^2\right]^{0.5}} \qquad (1)$$

$$z_0 = \frac{R_h}{1 + \left(\frac{\lambda R_h}{\pi (0.644a)^2}\right)^2} \qquad (2)$$

The beam radius at mirror 1 w_{m1} is given by equation (3). Here z_1 is the distance from the waist radius of the feed horn to the mirror. Equation (4) gives the beam waist radius between the two mirrors, where R_{i1} is the radius of curvature of the beam reflected off mirror 1. z_{12} given by equation (5) is the distance of the beam waist from mirror 1.

$$w_{m1} = w_0 \left[1 + \left(\frac{\lambda z_1}{\pi {w_0}^2}\right)^2\right]^{0.5} \qquad (3)$$

$$w_{m12} = \frac{w_{m1}}{\left[1 + \left(\frac{\pi {w_{m1}}^2}{\lambda R_{i1}}\right)^2\right]^{0.5}} \qquad (4)$$

$$z_{12} = \frac{R_{i1}}{1 + \left(\frac{\lambda R_{i1}}{\pi {w_{m12}}^2}\right)^2} \qquad (5)$$

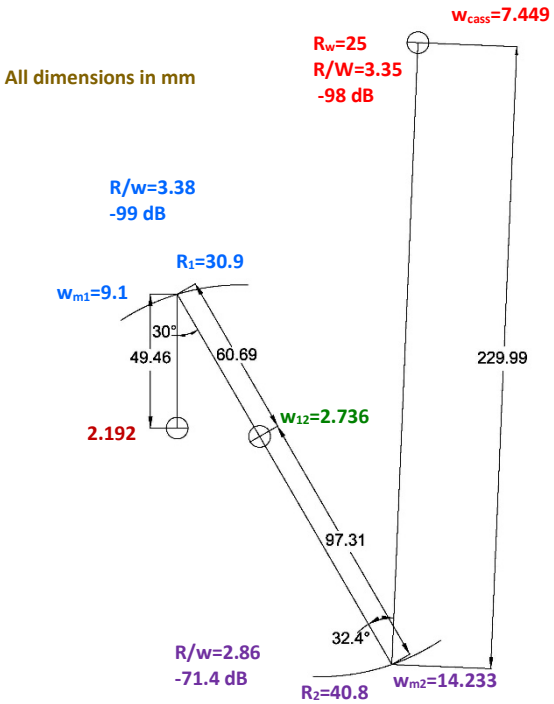

Figure 2. Beam radius at the mirrors and vacuum window.

In Table 1, R_{s1} is the distance from the focus F_1 (Figure 3) to the point of incidence on mirror 1, R_{i1} is the distance from the mirror to the other focus F_2, f_1 is the focal length and $\theta_1/2$ is the angle of incidence of the beam. These parameters and the diameter of the mirror define the ellipsoidal reflector and the section of the ellipsoid that is used. Figure 2 shows the beam radii at the mirrors, the beam waist of the feed horn, the waists in between the mirrors and at the secondary focus. The diameters of the mirrors 1 and 2 are 64 mm and 85 mm, respectively. The radii (R) of the mirrors projected perpendicular to the beam and the ratio R/W are also shown in the figure. The radii of the mirrors are 3.38x and 2.8x the beam radii at the mirrors. The edge taper is -99.0 dB and -71.4 dB for the two mirrors. The mirrors are sufficiently large not to cause any diffraction. The cross-polarization in the cartridge beam is caused mostly by the asymmetry of the mirrors. The vacuum window has a radius of 25 mm and given the beam radius at this location, the edge taper is -98.0 dB.

Physical optics analysis:

A rigorous EM simulation of the cartridge optics was carried out using the reflector analysis software GRASP (version 10.6.1) from TICRA. The feed horn is modeled using the "Hybrid Mode Conical Horn" option, which requires the input waveguide radius, the aperture radius and the semi flare angle. The phase center value is set at -3.464 mm. Figures 3 and 4 show the details of the ellipsoidal mirrors 1 and 2, respectively. The ellipsoidal mirror coordinate system is located at one of the foci F_2, with the z-axis pointed in the reflected beam direction. The ellipsoidal mirror is defined by the vertex distance, which is the distance between the two vertices (ellipsoidal major axis); the focal length, which is the distance between the foci; and the axis angle, which is the rotation angle of the axis about F_2. This angle is positive for a clockwise rotation of the z-axis towards the major axis, looking in the negative y direction. The usable part of the ellipsoid is the section with its concave side in the direction of the positive z-axis. The applied part of the ellipsoid is that defined by its rim. The parameters used in GRASP are indicated in Figures 3 and 4.

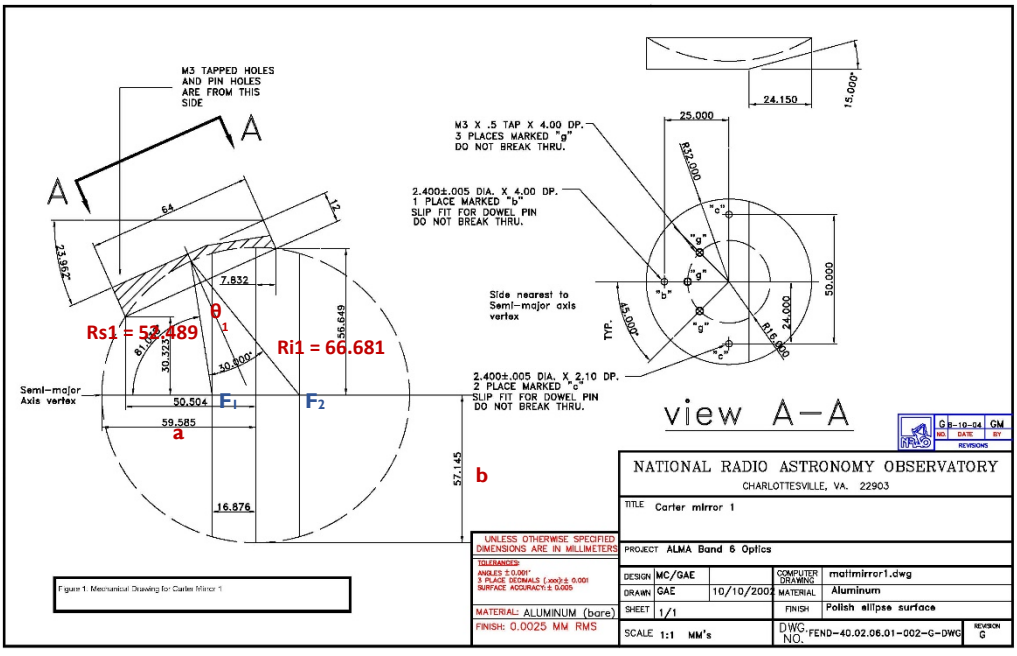

Figure 3. Details of mirror 1.

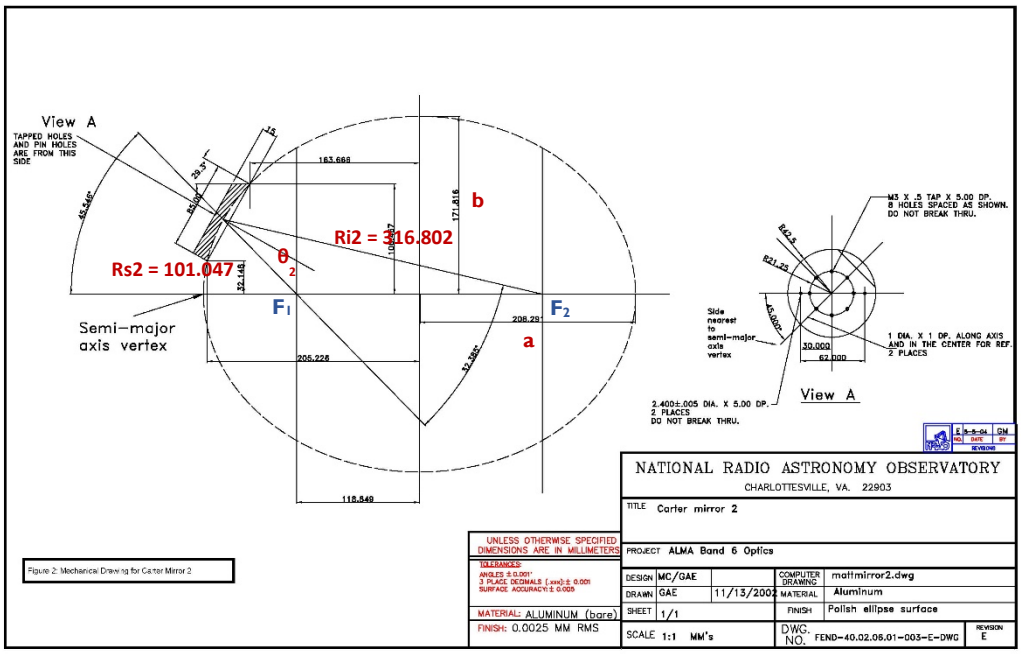

Figure 4. Details of mirror 2.

First a set of global coordinates referred to as “global_coord”, located at the Cassegrain focus of the antenna is defined and is shown in Figure 5. The coordinates of all the optical elements may be defined with respect to this coordinate system if it is convenient and easy.

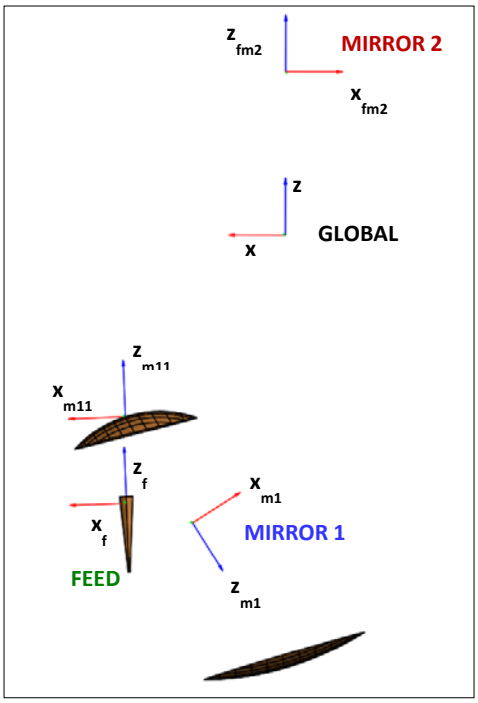

Figure 5. Coordinate system for the optical elements used in GRASP.

For the purpose of the intended analysis, a coordinate system located at the top of mirror 1 was chosen. This is referred as to "mirror11_coord". The z-axis of this coordinate system is aligned with the feed horn axis. The xz-plane of the coordinate system is in the symmetric plane of mirrors 1 and 2. The "mirror11_coord" is defined with respect to the "global_coord" system. The feed coordinate system "feed_coord" is located at the aperture of the feed horn. The coordinate systems for mirrors 1 and 2, referred to as "mirror1_coord" and "mirror2_coord", respectively, are located at one of foci of the respective ellipsoids, as mentioned earlier. All the above three coordinate systems shown in Figure 5 are defined with respect to "mirror11_coord" system. The far-field patterns of the quasi-optics are calculated with respect to the "global_coord" system, where the z-axis passes through the centers of the IR-filters, the cryostat window and subreflector, referred to as the optical axis.

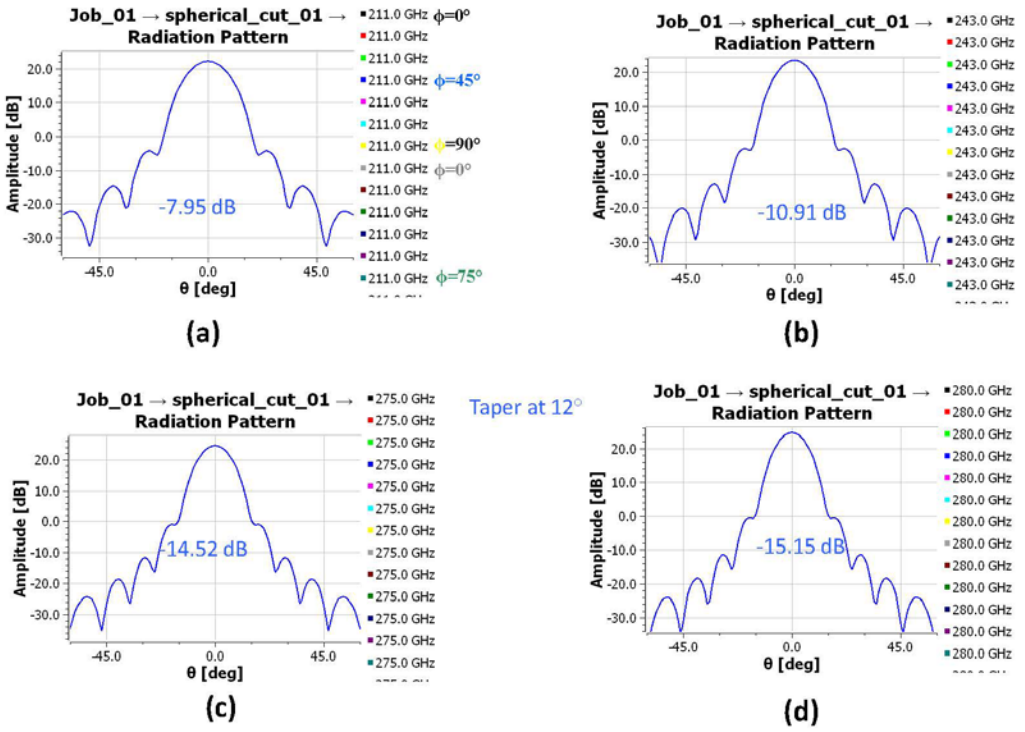

Figure 6. Far-field patterns hybrid-mode feed horn (a) 211 GHz, (b) 243 GHz, (c) 275 GHz, (d) 280 GHz. Cross-polarization is below -35dB

The far-field patterns of the hybrid mode feed horn are shown in Figure 6. These patterns calculated in GRASP agree closely with patterns of a corrugated horn calculated by mode matching technique shown in [4]. The co-pol and cross-polarized far-field patterns of the cartridge are shown in Figure 7 in seven planes from ϕ=0° to 90° spaced at 15° and at four frequencies. These patterns are in agreement with the measured beam patterns [5]. The ϕ=0° plane is the symmetric plane (xz-plane) and ϕ=90° plane is the asymmetric plane (yz-plane, orthogonal to the symmetric plane). The illumination taper at 3.58° (the

edge angle of the subreflector) is shown in the figure and varies between -12.4 dB and -12.6 dB. Cross-polarization lobes are also shown and the maximum is at 211 GHz (-31.6 dB) in the ϕ=90° plane.

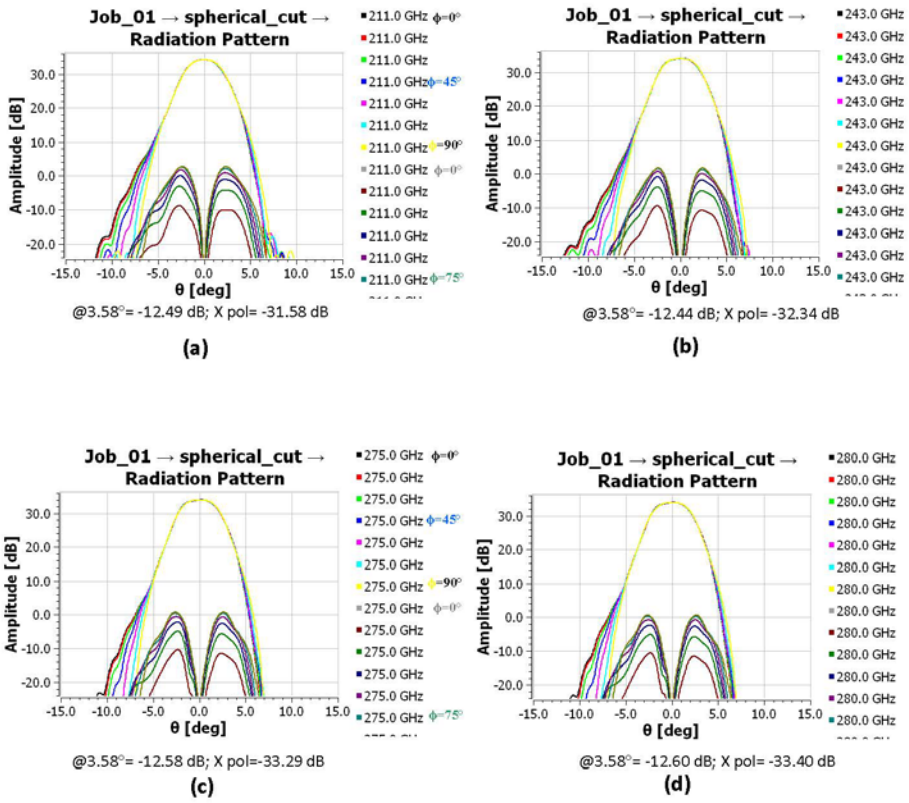

Figure 7. Far-field patterns of the Band-6 cartridge ϕ=0° to 90° spaced at 15° (a) 211 GHz, (b) 243 GHz, (c) 275 GHz, (d) 280 GHz.

Feed horn position errors:

The feed horn is mounted on a brace that is secured to the A-frame at three locations as shown in Figure 1(a). Positional errors can be mainly in the x- and y-axis and three cases considered are +x, -x and +y. The feed position is varied with respect to "mirror11-coord" in x and y directions and far-field patterns are calculated about the "global_coord" system.

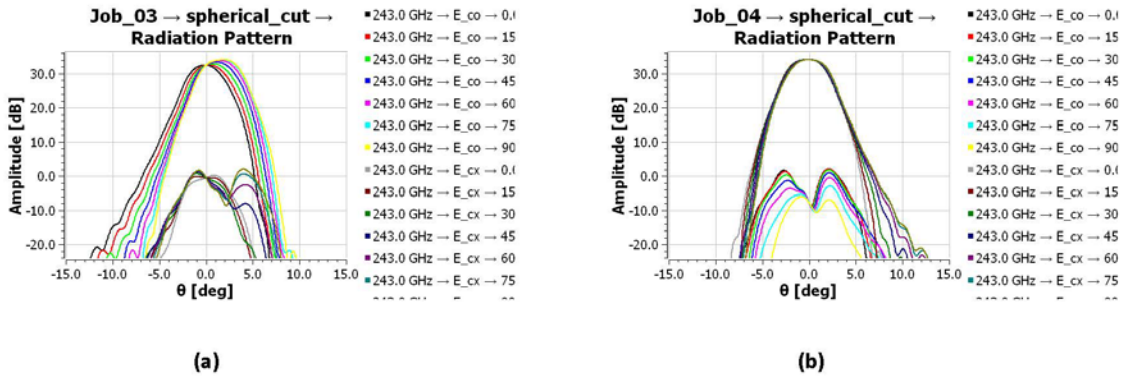

Figure 8. Far-field patterns for feed positional error of y=1.234 mm (a) Cuts along the optical axis, (b) Cuts along the beam maximum.

Figure 8(a) shows co-pol and cross-polarization patterns at 243 GHz in planes spaced 15° apart, for a positional error of y=1.234 mm (1λ at 243 GHz). Only the pattern in ϕ=90° (yellow trace) goes through the peak of the beam and is offset from the optical axis by 1.9° (β). Figure 8(b) shows the pattern cuts centered about the peak of the beam offset in the asymmetric plane. The location of the feed and the beam direction for an offset of 1.234 mm in x, -x and y directions are shown in Figure 9. The beam scan angles are -1.85°, 1.80° and 1.90° for the three cases, respectively.

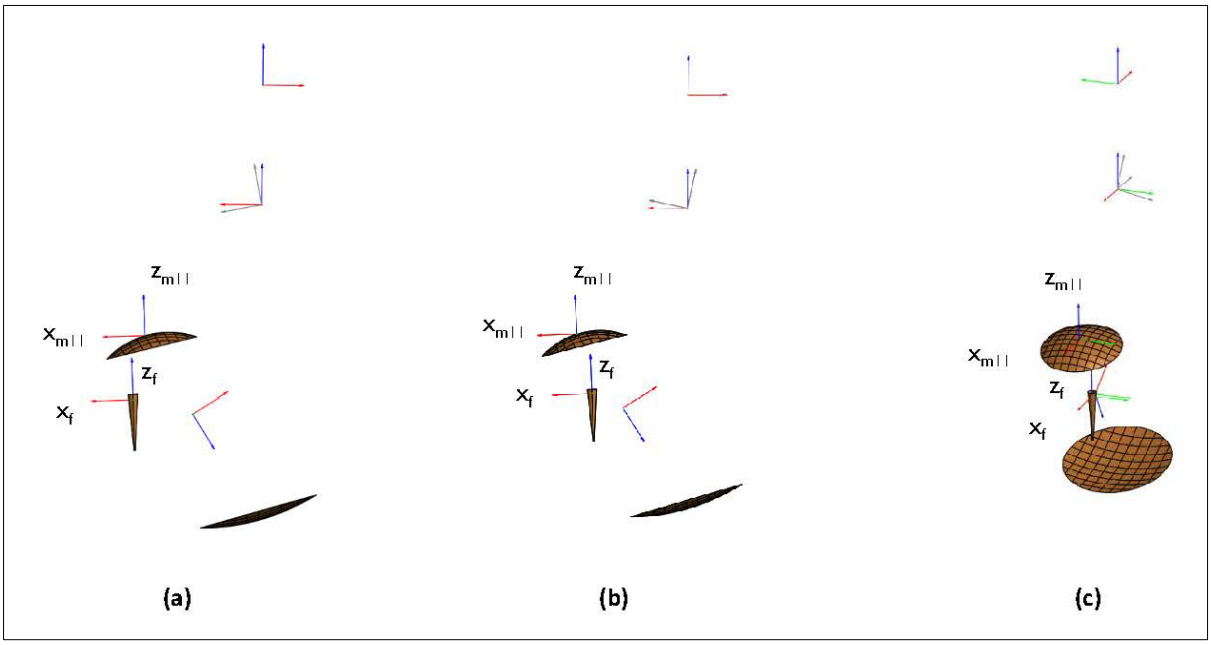

Figure 9. Feed positional errors with direction of beam maximum in global coordinates (gray) (a) x= 1.234 mm, (b) x= -1.234 mm, (c) y=1.234 mm.

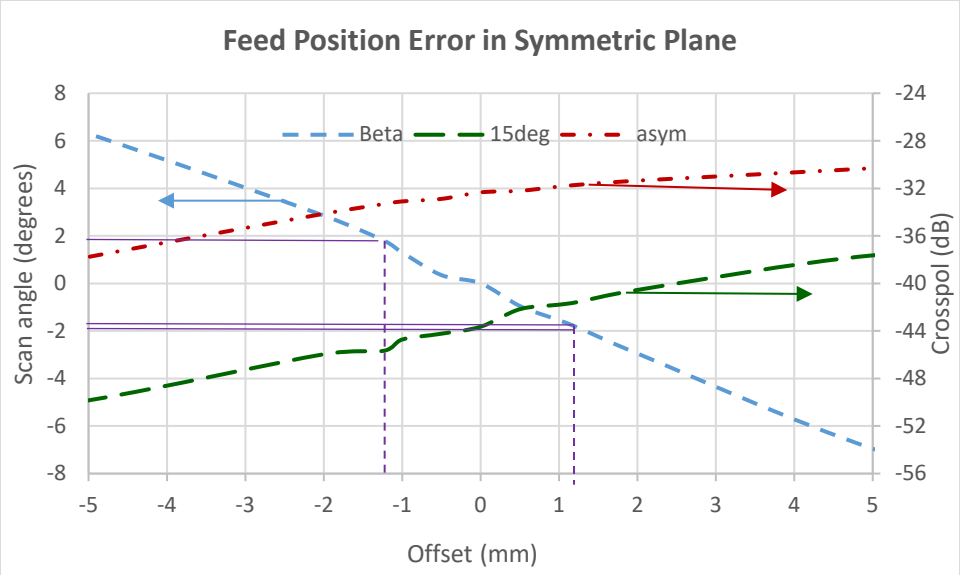

(a)

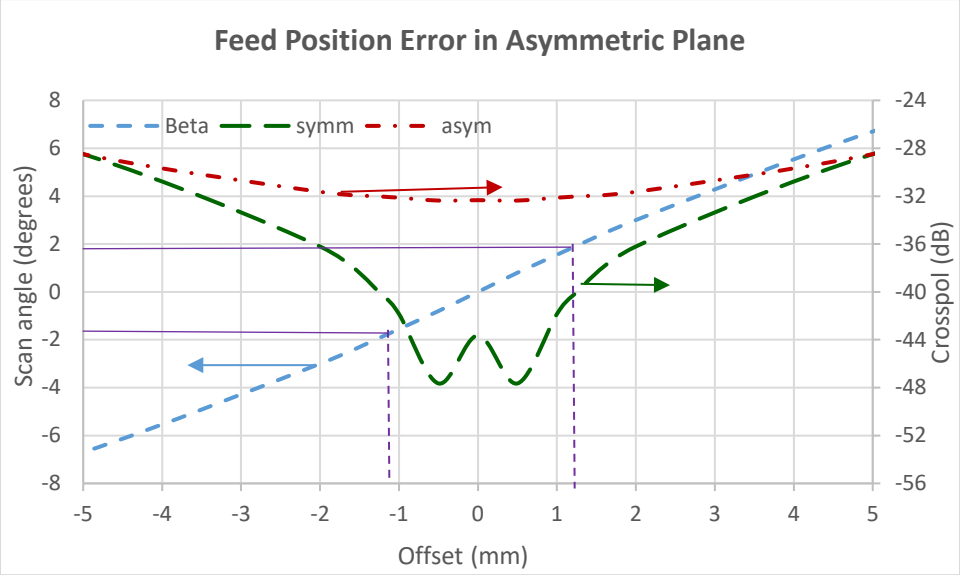

(b)

Figure 10. Scan angle, Cross-polarization Vs. Feed position error (a) Symmetric Plane, (b) Asymmetric plane.

Figure 10(a) shows the scan angle in the symmetric plane and level of cross-polarization in ϕ=15° and 90° planes as a function of feed offsets up to ±5mm in the x- direction. Cross-polarization in the symmetric plane (ϕ=0°) is below -100 dB. The purple horizontal lines are at scan angles of ±1.79° (half of the subreflector angle), where the feed offsets are about 1.2 mm. Cross-polarization in the asymmetric plane is better than -32 dB at 1.79°, worse by about -1 dB compared to that for the nominal feed positon. Figure 10(b) shows the scan angle in the asymmetric plane and level of cross-polarization in the asymmetric and symmetric planes for feed offset in the y-direction. Notice that the cross-polarization levels in the symmetric plane have become much worse and are at about the same level as the ϕ=15°

levels in Figure 10(a). Cross-polarization in the asymmetric plane is again worse compared to that for offsets in the x-direction. The scan angles are about the same for both cases except the sign reversal.

Mirror 1 position and angular errors:

The cross-polarization and beam scan sensitivity to positional and rotational offsets of mirror 1 is presented in this section. Figure 11 shows the far-field patterns at 243 GHz for a positional error of 1.234 mm of mirror 1 in the y-direction, along the optical axis and along the beam maximum. The beam scan angle in this case is -2.90° in the asymmetric plane. The position of mirror 1 and the beam direction are shown in Figure 12, for offsets of 1.234 mm in the x, -x and y directions in the mirro11_coord system. The beam scan angles are 2.75°, -2.65° and -2.90°, respectively for the three cases. The scan angle and cross-polarization level as a function of mirror 1 positional errors in the x-direction are shown in Figure 13(a). The slope of the scan angle curve is steeper compared to the feed horn offsets. However, the deterioration of cross-polarization is smaller. The positional error sensitivity in the y-direction is shown in Figure 13(b). The scan angle slope is steeper again compared to the feed horn case. Cross-polarization in the asymmetric plane is about the same level for errors up to 1.5 mm, and gets worse faster and is about -25 dB for an error of 5 mm. Cross-polarization in the symmetric plane is worse for most of the offsets, compared to the feed offsets. Rotation of mirror 1 about the z-axis was analyzed as this is plausible if the mounting holes on the A-bracket are slightly out of position. Figure 13(c) shows the sensitivity curves for rotational angles up to 5°. The slope of the beam rotation is very nearly linear and has a slope of 0.6. The cross-polarization sensitivity is smaller compared to the positional error cases.

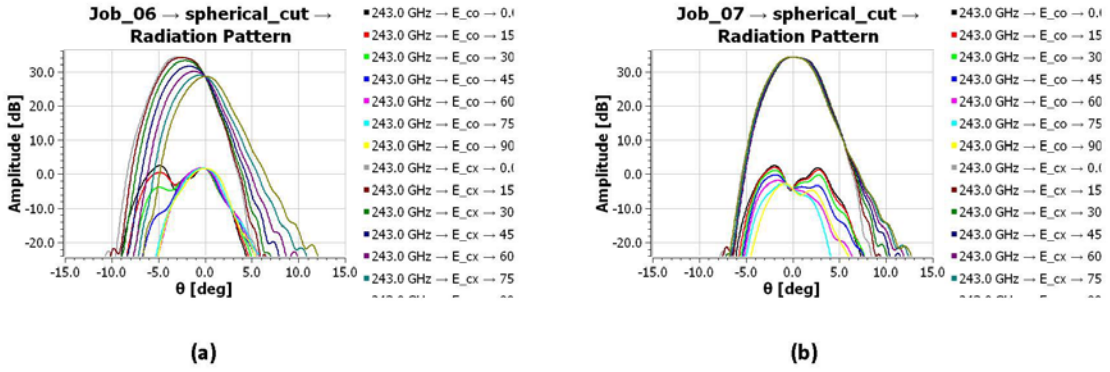

Figure 11. Far-field patterns for mirror 1 positional error of y=1.234 mm (a) Cuts along the optical axis, (b) Cuts along the beam maximum.

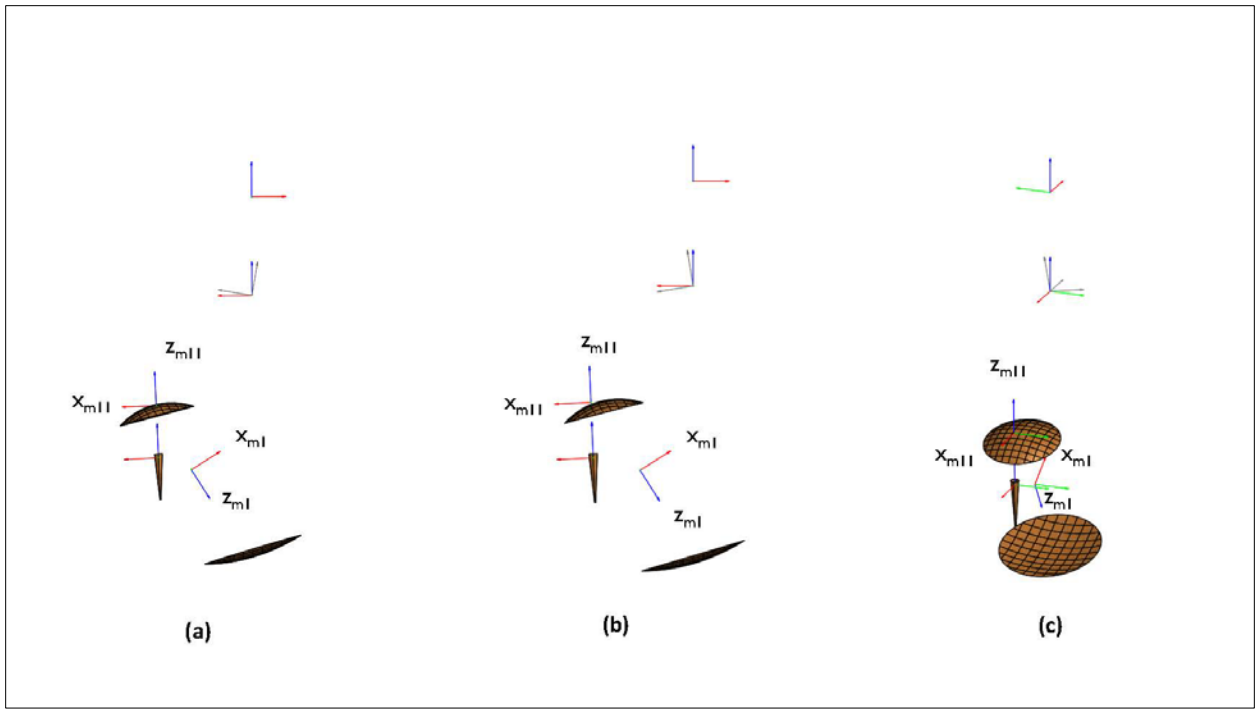

Figure 12. Mirror 1 positional errors with direction of beam maximum in global coordinates (gray) (a) x= 1.234 mm, (b) x= -1.234 mm, (c) y=1.234 mm.

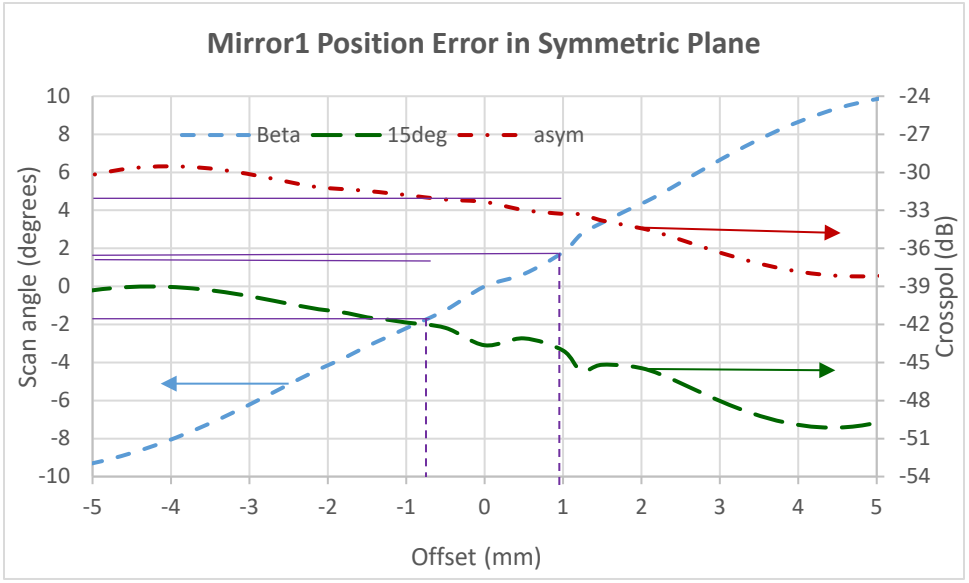

(a)

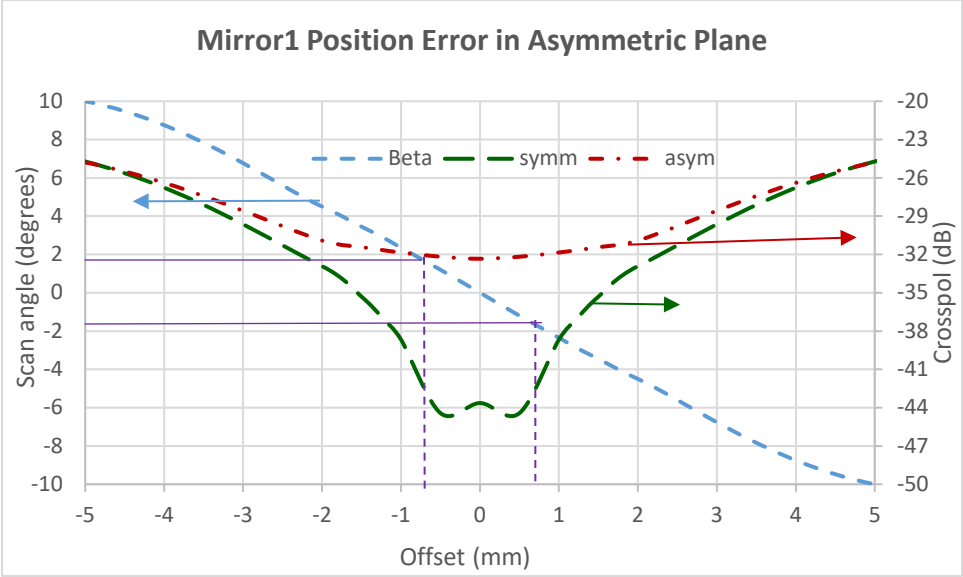

(b)

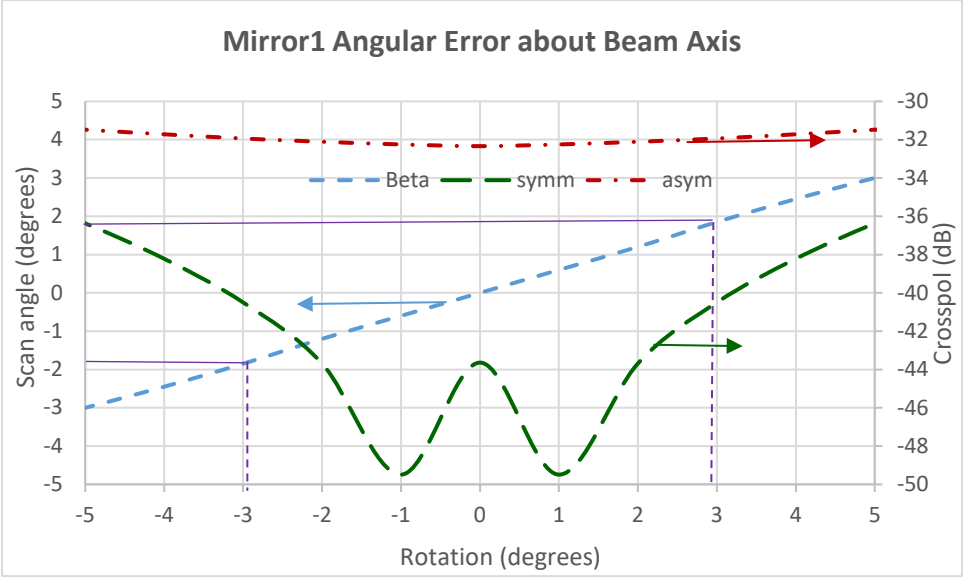

(c)

Figure 13. Scan angle, Cross-polarization Vs. (a) Position error in Symmetric Plane, (b) Position error in Asymmetric plane, (c) Rotation about central axis for mirror 1.

Mirror 2 translations and rotation:

The effects of linear and rotational offsets of mirror 2 from its nominal position have also been analyzed. Figure 14(a) shows beam patterns along the optical axis at 243 GHz and Figure 14(b) shows beam patterns along the beam maximum for an offset of 1.234 mm of mirror 2 in the y-direction.

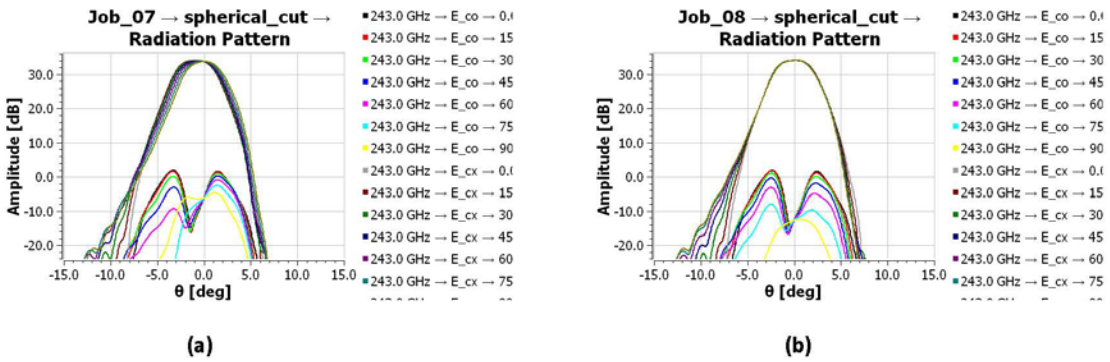

Figure 14. Far-field patterns for mirror 2 positional error of y=1.234 mm (a) Cuts along the optical axis, (b) Cuts along the beam maximum.

Figure 15 shows positions of mirror 2 and beam scan directions, for offset of 1.234 mm in the x, -x and y directions. The scan angles for the three cases are -1.05°, 0.45° and 0.95°, respectively.

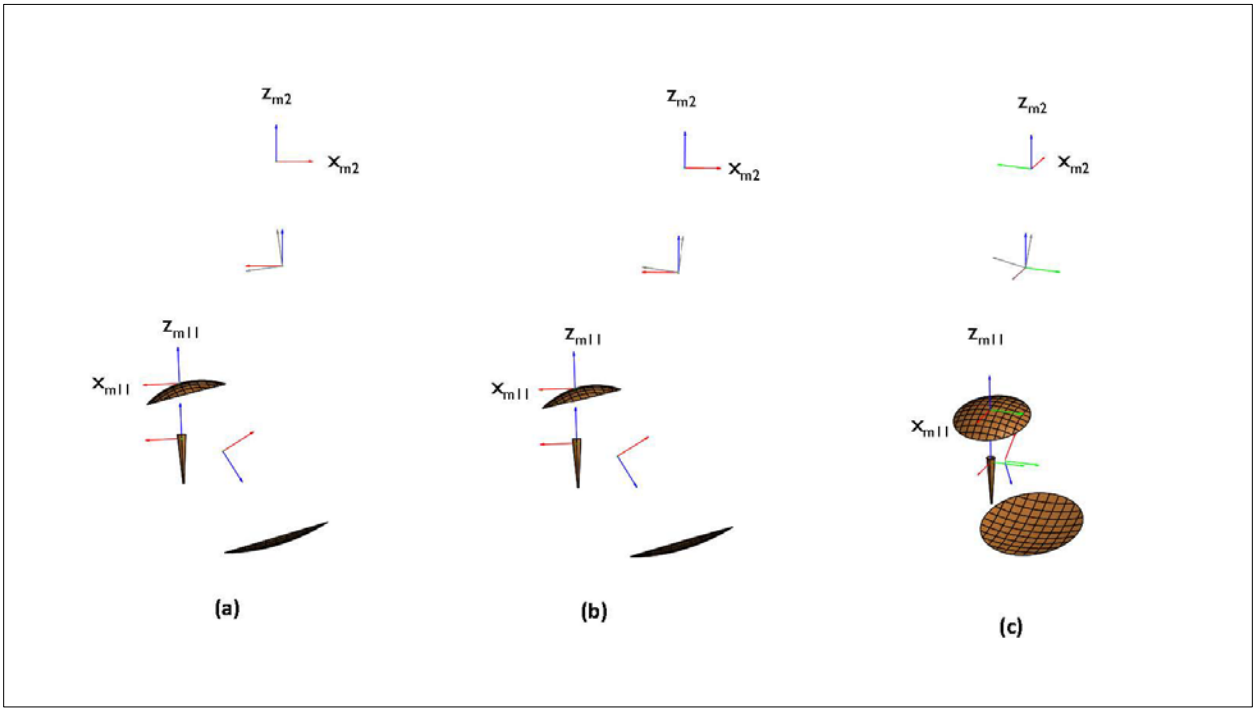

Figure 15. Mirror 2 positional errors with direction of beam maximum in global coordinates (gray) (a) x= 1.234 mm, (b) x= -1.234 mm, (c) y=1.234 mm.

The sensitivity for offsets in the x-direction is shown in Figure 16(a). The slope of the scan angle is asymmetric, more sensitive for positive offsets. The beam scan is much smaller, about 30% compared to that of the case mirror 1. Deterioration of cross-polarization is small compared to the other two cases.

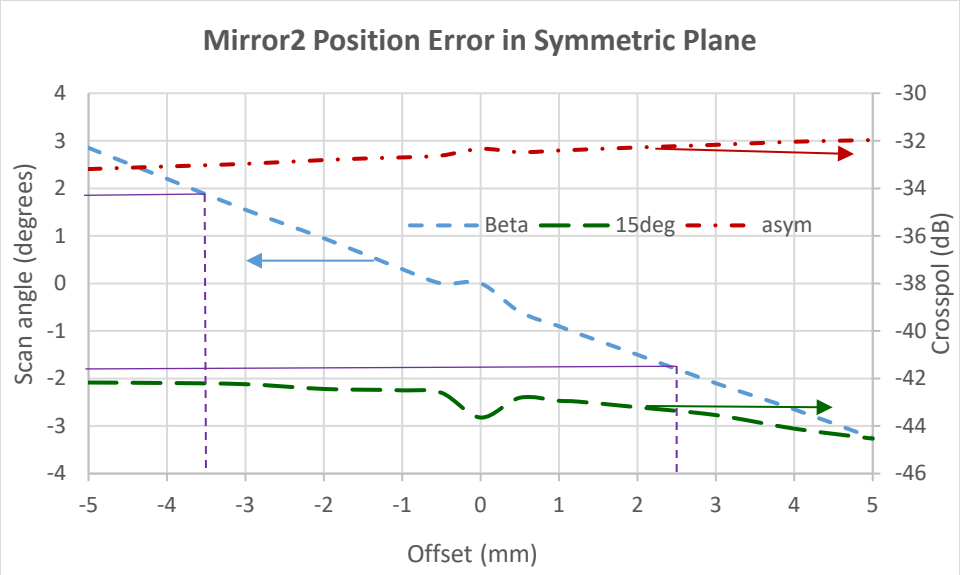
Mirror2 Position Error in Symmetric Plane
Scan angle (degrees)
Crosspol (dB)
Offset (mm)
Beta
15deg
asym
4
3
2
1
0
-1
-2
-3
-4
-30
-32
-34
-36
-38
-40
-42
-44
-46
-5
-4
-3
-2
-1
0
1
2
3
4
5

(a)

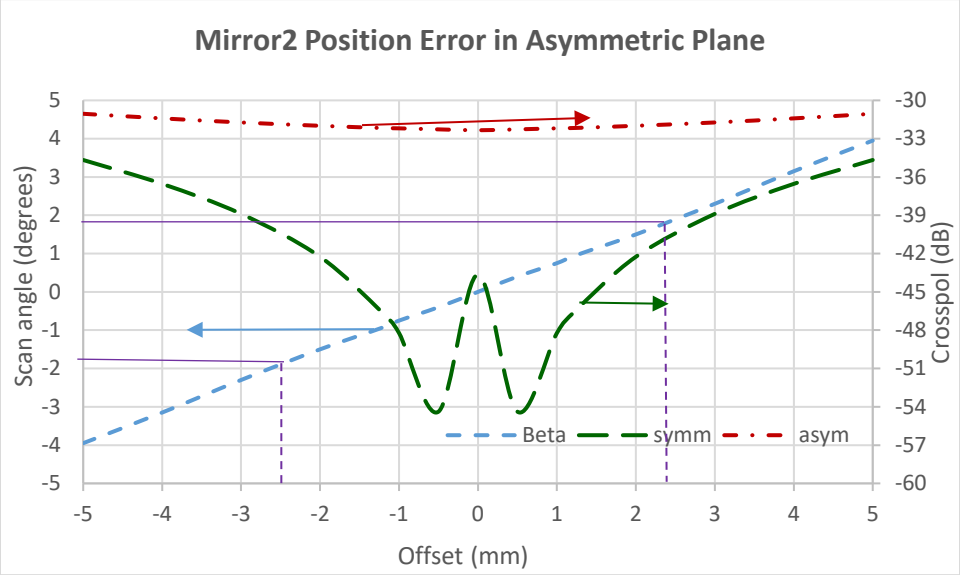
Mirror2 Position Error in Asymmetric Plane
Scan angle (degrees)
Crosspol (dB)
Offset (mm)
Beta
symm
asym
5
4
3
2
1
0
-1
-2
-3
-4
-5
-30
-33
-36
-39
-42
-45
-48
-51
-54
-57
-60
-5
-4
-3
-2
-1
0
1
2
3
4
5

(b)

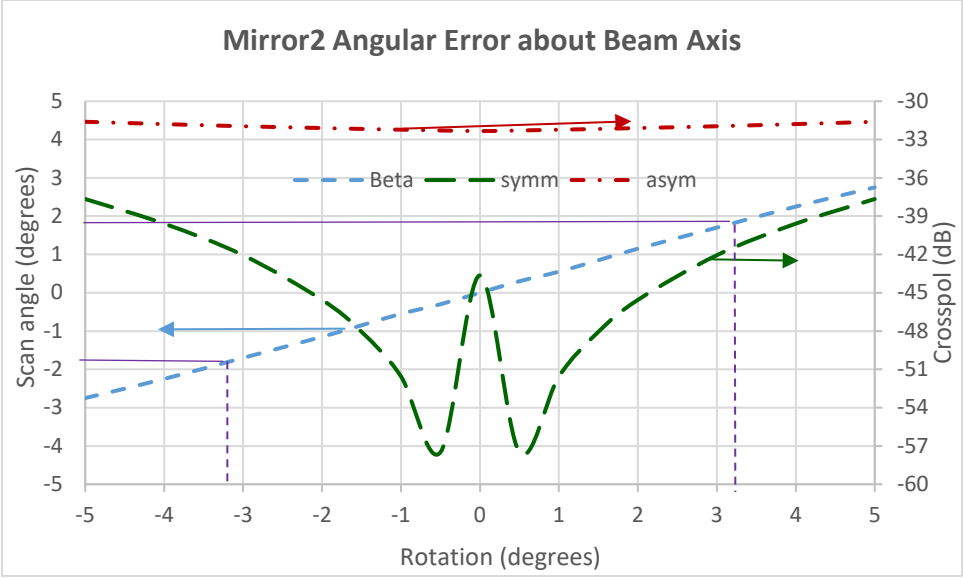

(c)

Figure 16. Scan angle, Cross-polarization Vs. (a) Position error in symmetric Plane, (b) Position error in asymmetric plane, (c) Rotation about central axis for mirror 2.

Figure 16(b) shows sensitivity for offsets in y-direction. The scan angle sensitivity is higher compared to the corresponding offset for mirror 1 and much lower compared to the feed case. Figure 16(c) shows sensitivity of beam scan for rotations about the z-axis and is minutely smaller compared to mirror 1 rotation. Cross-polarization variation is very similar to that for mirror 1.

Conclusions:

Gaussian beam propagation through the optical elements of the Band-6 cartridge has been analyzed. The beam radii were calculated at the location of the mirrors and the first IR filter. The size of the mirrors/filter is at least 2.9x the beam radius. The power level at the edges is lower than -71 dB, indicating that there is no diffraction caused by the edges. The sizes of the mirrors are sufficiently large that they do not cause any diffraction. A future study could cover the effect of reducing the size of the mirrors in order to reduce thermal loading, without any sacrifice in performance.

The deterioration in cross-polarization is very small for offsets of the feed or the ellipsoidal mirrors from their nominal positions, before the beam scan reaches half of the subreflector subtended angle. The beam scan is most sensitive to linear offsets of mirror 1 in both the symmetric and asymmetric planes. Rotation of mirror 1 and mirror2 have similar effects on the beam scan and cross-polarization. The positional tolerances specified for the optical elements are extremely tight resulting in very small beam scan and absolutely no effect on the level of cross-polarization. The effect of the IR filters and vacuum window on cross-polarization was not studied in this analysis.

References:

[1] J. Carpenter, D. Iono, L. Testi, N. Whyborn, A. Wotten, N. Evans, “The ALMA Development Roadmap”.

[2] S. Asayama, G. Han Tan, K. Saini, J. Carpenter, G. Siringo, T. Hunter, N. Phillips, H. Nagai, "Report of the ALMA Front-end & Digitizer Requirements Upgrade Working Group”, ALMA-05.00.00.00.0048-A-REP, Ver. B, 16 Dec. 2020.

[3] A. Navarrini et al., “ALMA Band 6v2 Receiver Upgrade: Phase 1”, Development Upgrades of the Atacama Millimeter/submillimeter Array, July 16, 2021.

[4] C. Y. Tham, S. Withington, “The Atacama Large Millimetre Array – Receiver Optics Design Electromagnetic Analysis”, Cavendish Laboratory, University of Cambridge, UK, July 1, 2003.

[5] “Measured Beam Patterns for CCA6-046”, CDL document, December 15, 2020.

Table 1. Parameters of the optical elements, Quasi-optics Gaussian beam parameters

Frequency (GHz)		**211**	**243**	**275**
λ (mm)		1.420817	1.233714	1.090154
Horn diameter	7.08			
Horn axial length	46.5373			
Horn slant length	46.6717			
Horn waist, w_0		2.212	2.192	2.169
Horn waist offset, $\Delta z(w_0)$		-2.6601	-3.4637	-4.3454
Waist at horn aperture, w_{ha}		2.278	2.278	2.278
d_1	46.00			
R_{s1}	52.489	51.066	52.489	53.999
f_1	29.37			
R_{i1}	66.681	69.128	66.681	64.394
Waist at mirror 1, w_{M1}	(dia. = 64)	10.191	9.129	8.340
θ_1	30.0°			
z_{w1}		63.3852	60.6897	58.3706
w_1		2.938	2.736	2.551
d_2	158.00			
R_{s2}	101.047	98.462	101.047	103.158
f_2	76.611			
R_{i2}	316.802	345.210	316.802	297.697
Waist at mirror 2, w_{M2}	(dia. = 85)	14.860	14.230	13.791
θ_2	32.3848°			
$z_{w(Cass.)}$	230.0	230.162	229.996	229.884
$w_{Cass.}$		8.579	7.449	6.582
$d_{mirror\text{-}subrefl}$		6225.75	6226.67	6227.28
$w_{subrefl}$	(dia. = 750)	316.197	316.224	316.243
$R_{subrefl}$	6000.00	6000.000	6000.000	6000.000
Multimode truncation (dB)	10.00	9.99	10.00	9.99
Edge Taper (dB)	12.00	12.22	12.21	12.21

Dimensions in mm.

θ_2